Available online at www.sciencedirect.com
SCIENCE DIRECT
Biochimica et Biophysica Acta 1711 (2005) 59–71
BIOCHIMICA ET BIOPHYSICA ACTA
BBA
http://www.elsevier.com/locate/bba

Raman spectra of planar supported lipid bilayers

Chongsoo Lee, Colin D. Bain*

Department of Chemistry, University of Oxford, Chemistry Research Laboratory, Mansfield Road, Oxford OX1 3TA, United Kingdom

Received 23 December 2004; received in revised form 9 February 2005; accepted 9 February 2005
Available online 19 March 2005

Abstract

Raman scattering has been used to obtain high quality vibrational spectra of planar supported lipid bilayers (pslb's) at the silica/water interface without the use of resonance or surface enhancement. A total internal reflection geometry was used both to increase the bilayer signal and to suppress the water background. Polarization control permits the determination of four components of the Raman tensor, of which three are independent for a uniaxial film. Spectra are reported of the phospholipids DMPC, DPPC, and POPC, in the C–H stretching region and the fingerprint region. The temperature-dependent polarized spectra of POPC show only small changes over the range 14–41 °C. The corresponding spectra of DMPC and DPPC bilayers show large thermal changes consistent with a decreasing tilt angle from the surface normal and increasing chain ordering at lower temperatures. The thermal behavior of DMPC pslb's is similar to that of vesicles of the same lipid in bulk suspension. In contrast to calorimetry, which shows a sharp phase transition (L_α–$L_{\beta'}$) with decreasing temperature, the changes in the Raman spectra occur over a temperature range of ca. 10 °C commencing at the calorimetric phase transition temperature.

Keywords: Total internal reflection; Raman spectroscopy; Phase transition; Planar supported lipid bilayer; Dimyristoyl phosphatidylcholine; Dipalmitoyl phosphatidylcholine

1. Introduction

Raman spectroscopy has a long history in biophysical chemistry [1–4]. All molecules of biological interest have vibrational spectra, which are often sensitive to conformation, secondary structure and to weak intermolecular interactions [2,5–7]. Water absorbs very strongly in the mid-infrared region of the electromagnetic spectrum, but scatters light only weakly, so Raman spectroscopy is often the vibrational spectroscopy of choice for studying biomolecules in a native aqueous environment. Raman scattering, however, is a weak effect (scattering cross-sections are typically 12–14 orders of magnitude weaker than for fluorescence [2]) and is easily swamped by competing photophysical processes. Many different types of Raman spectroscopy have been applied to overcome these limitations, including FT-Raman [8,9], UV resonance Raman (UVRR) [1], surface-enhanced Raman (SERS) [10], coherent anti-Stokes Raman (CARS) [11,12], and Raman optical activity (ROA) [13].

This paper is concerned with the study of the planar supported lipid bilayers under water. Raman scattering is particularly useful for studying fluidity and conformational order in lipid mesophases [14–17], but the low sensitivity of Raman scattering has largely precluded its use for studying single lipid bilayers. If one wishes to mimic the function of the outer cellular membrane it is essential that the bilayer is unilamellar and immersed in an aqueous environment. While single-bilayer sensitivity could be achieved by SERS, adsorption on a roughened metal surface may seriously compromise membrane function. We demonstrate here that single supported lipid bilayers can be studied by conventional, non-resonant Raman scattering by taking advantage of the properties of evanescent waves. The use of total internal reflection (TIR) geometry to deliver the pump laser beam also affords a larger range of polarization combinations than are accessible in studies of bulk samples or with confocal Raman microscopes. This additional information is

* Corresponding author. Tel.: +44 1865 275467; fax: +44 1865 285002.
E-mail address: colin.bain@chem.ox.ac.uk (C.D. Bain).

0005-2736/$ - see front matter © 2005 Elsevier B.V. All rights reserved.
doi:10.1016/j.bbamem.2005.02.006

a valuable aid for structure determination. To illustrate the use of this technique, we present a study of the main phase transition of planar supported lipid bilayers (pslb) of dimyristoyl phosphatidylcholine (DMPC) and dipalmitoyl phosphatidylcholine (DPPC) and compare the behaviour of the pslb's with the same lipids in a suspension of a lamellar mesophase. The Raman spectra of pslb's of the partially unsaturated lipid, palmitoyl oleoyl phosphatidylcholine (POPC), are shown for comparison.

2. Materials and methods

2.1. Materials and sample preparation

POPC from egg yolk, DMPC, and DPPC were purchased from Sigma Chemicals (St. Louis, MO, USA). Planar supported lipid bilayers of POPC, DMPC, and DPPC were prepared by the fusion of small unilamellar vesicles (SUVs) onto a fused silica window [19,44]. The individual lipids were first dissolved in chloroform, evaporated to dryness on a rotary evaporator and then hydrated in 10 mM Tris buffer containing 100 mM NaCl at pH 8.0 in a bath sonicator (Langford 475H, Langford Ultrasonics, Warwickshire, UK) at 60 °C for 2 h, to give 2-mM suspensions of multistacked lipid films. The suspensions were then ultrasonicated with fifty 1-min bursts at 25% of the total power, keeping the rise in temperature (T) to less than 10 °C (Model VC505, Jencons Ltd., Bedfordshire, UK) [18,19]. The resulting transparent vesicle solutions containing multilamellar, large unilamellar, and single unilamellar vesicles were ultra-centrifuged under 166,000 g for 1 h. And the supernatant extracted, resulting in a solution containing only SUVs. The average hydrodynamic diameter of the SUVs was evaluated to be 35 nm by photocorrelation spectroscopy, consistent with the formation of SUVs. To form pslb's, 100-μL aliquots of SUV solution (ca. 0.2 mg/ml in the same buffer solution) were placed on a fused silica window and covered by a coverslip. The solution was allowed to incubate with the silica surface for 45 min at Ts of 30 °C for DMPC, 45 °C for DPPC, and 18 °C for POPC. An additional buffer was placed at the edge of the coverslip to prevent evaporation of the vesicle solution. The coverslip was then removed by the addition of further buffer and the silica window gently rinsed at least 10 times with copious amounts of ultra high quality (uhq) water (≥18 MΩ cm) to remove excess vesicles that have not been fused to the silica surface. The planar supported lipid bilayers were then immersed in uhq water. Exposure of the lipid to the air was minimized. A vesicular suspension of DMPC was prepared by the same buffer hydration described above but with bath sonication for 3 h at 60 °C. Tapping-mode AFM was used to confirm that the vesicles of POPC had fused to the silica surface. After very short exposure times (1 min) 'doughnut' shapes with a typical diameter of 50 nm were observed on the surface, which may represent flattened vesicles that have not yet fused to the silica. With continuing exposure to the vesicle solution, these features disappeared and the surface became progressively flatter. After 10 min exposure, the surface appeared featureless with an rms roughness of 2.5 Å.

2.2. Polarized TIR Raman microscopy

Raman spectra were collected with a commercial Raman microscope (Renishaw System 1000, Wotton-under-Edge, U.K.) equipped with a ×40, water-immersion objective (Zeiss). The pump laser was a 2-W frequency-doubled diode-pumped YVO_4 laser (Spectra-Physics Millennia 2) delivered externally to the microscope (see Fig. 1A). Except where stated otherwise, the nominal power (at the laser head) was 1.2 W, corresponding to approximately 0.8 W at the sample. The angle of incidence at the silica–water interface was approximately 68.6°, compared to the critical angle of 65.8°, giving a penetration depth of around 77 nm. The laser spot was ellipsoidal with a typical size of 80 μm×40 μm with s-polarized excitation (60 μm×30 μm with p-polarized excitation). The width of the slit before the

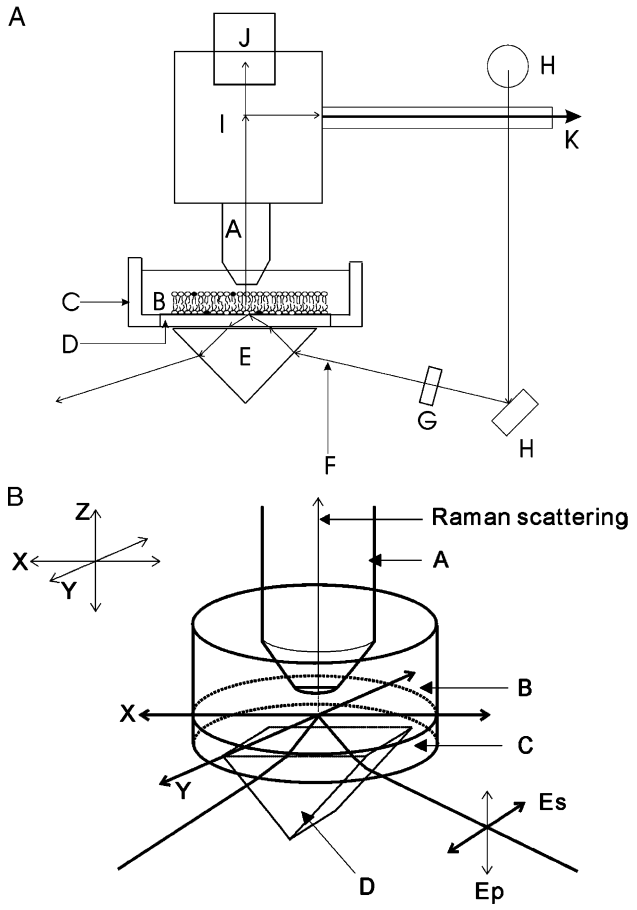

Fig. 1. (A) Schematic diagram of total internal reflection Raman (TIR) spectroscopy (A: objective lens; B: buffer solution; C: PTFE sample dish; D: fused silica window; E: boron silicate prism; F: incoming laser beam; G: lens; H: mirror; I: microscope; J: CCD camera; K: optical path to monochrometer and CCD detector). (B) Definition of laboratory coordinates and polarization directions defined for TIR Raman experiment.

spectrometer was 200 μm and 11 pixels on the CCD chip were binned together in the direction perpendicular to the wavenumber axis. The definitions of the polarization of the excitation (s or p) and of the detected light (x or y) are shown in Fig. 1B.

2.3. Measurement of phase transitions in pslb's

The housing of the sample cell was constructed from brass and thermostatted with flowing liquid to ±0.1 °C. The *T* of the sample was measured with a thermocouple placed on the silica window as close as possible to the point of illumination of the laser beam. There was no measurable increase in the *T* of the buffer following extended laser illumination.

2.4. Measurement of phase transitions in bulk suspensions of vesicles

The spectra of the bulk suspension of DMPC vesicles were recorded in capillary tubes (1-mm diameter, ~2 mM lipid) in a *T*-controlled cell, using the internal beam path of the Raman spectrometer. The pump beam was focused to a 2-μm diameter spot just below the inner wall of the capillary to minimize light scattering from larger aggregates in the suspension. The *T* was measured with a thermocouple placed adjacent to the capillary tube. The nominal power was 30 mW. No polarization selection was applied to the backscattered light.

2.5. Sample heating and damage

To test whether the pump laser caused significant heating of the lipid bilayer, we compared the spectra of DMPC bilayers at 0.3 W increments in the nominal power from 0.3 W to 1.5 W at a temperature of 22 °C. A similar experiment was performed on bulk vesicles at 22.5 °C with nominal powers, after attenuation by ND filters, between 6 and 30 mW. These are *T* where the Raman spectra are sensitive to small changes in *T*. Within each series, the spectra were indistinguishable to within a scale factor arising from the different power levels. We conclude that the pump laser causes no significant heating of the lipid film. To test for sample damage, consecutive Raman spectra were acquired for 30 min each on the same area of the surface. No change in the lipid spectrum was observed.

3. Results

3.1. Raman difference spectra

Modern Raman microscopes are usually used in a backscattering, confocal geometry where the pump beam is delivered and the Raman light collected through the same objective. While this geometry could be used to study pslb's in a buffer, there is no intrinsic surface sensitivity. While the Raman scattering cross-section of water is weak relative to the lipid, the water is in vast excess. Even with a high numerical aperture objective and a small collection slit, there are 10^4 water molecules contributing to the spectrum for each lipid molecule. Rather than focusing the pump laser beam through the collection optics, we deliver the beam externally through the silica substrate (Fig. 1). A coupling prism is used to ensure that the pump laser is just above the critical angle for TIR at the silica–buffer interface. An evanescent electric field penetrates about 100 nm into the buffer, decreasing exponentially away from the silica surface. It is this field that excites Raman scattering from the fused lipid bilayer. The scattered light is collected by a high numerical aperture water-immersion objective. Fig. 2 shows raw Raman spectra of a clean silica window

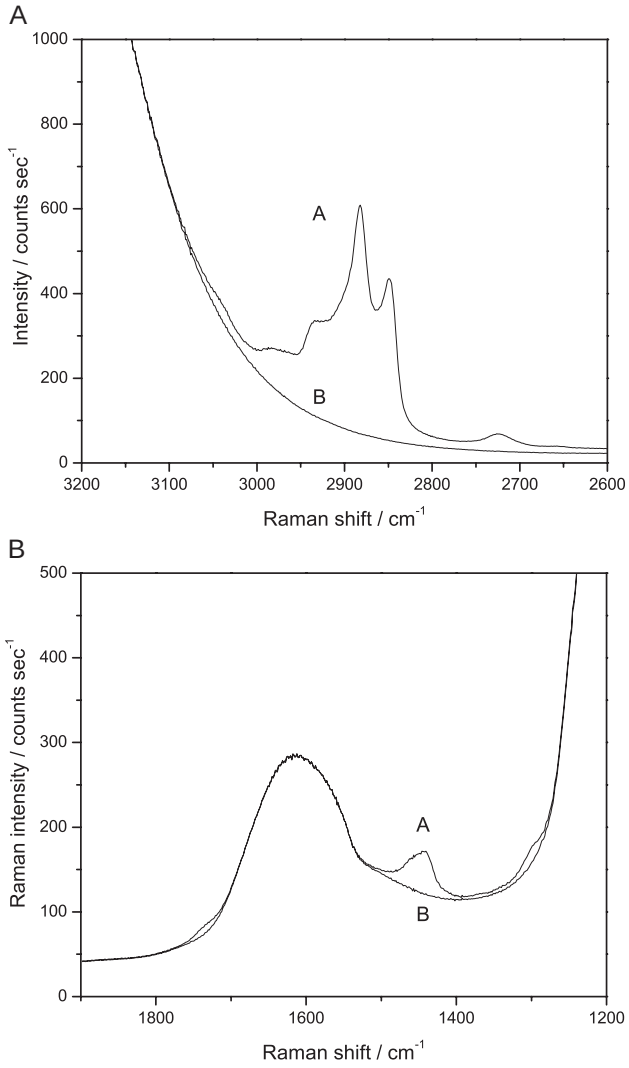

Fig. 2. Raman spectra of (A) planar supported DPPC bilayer in water at 32.8 °C and (B) pure water in the (A) C–H stretching region and (B) fingerprint region (1.2 W, s-polarized excitation, no polarization selection in detection, acquisition time=450 s). All subsequent spectra are shown after the subtraction of water background.

(reference) and a silica window coated with a bilayer of DPPC (sample) both in contact with pure water. In both the C–H stretching region (Fig. 2A) and the fingerprint region (Fig. 2B) the water background in the sample spectrum is well-matched in the reference spectrum. All subsequent spectra are shown after the subtraction of a water reference. Since the lipid bilayer displaces water, there is no reason why there should be an exact match in water contributions to the sample and reference spectra. Consequently, a variable subtraction factor was employed to generate the flattest baseline: In Fig. 2A, the factor was 0.994. Essentially a perfect subtraction of the O–H stretching and bending modes can be achieved. The only consequence of the water in the spectrum is increased noise in the regions of the water bands (compare 3100 cm^{-1} and 2600 cm^{-1} in Fig. 4A). The region below 1200 cm^{-1} is obscured by the Si–O stretches of the substrate. If this region is of particular interest (e.g. to detect phosphate vibrations) a different substrate lacking vibrations at these frequencies could be chosen.

3.2. Confirmation of pslb's

To establish that we are observing single lipid bilayers, and not multilamellar films, we compared the spectral intensities from pslb's of POPC, DMPC and DPPC with a silica surface exposed to a solution of the surfactant hexadecyltrimethylammonium bromide (C_{16}TAB) at a concentration just above the critical micelle concentration (cmc=0.92 mM) (Fig. 3). It is known from the work of Atkin et al. [24] that C_{16}TAB adsorbs onto silica with a surface excess of 4.4 μmol m^{-2} at 24.5 °C. If we make the crude assumption that the integrated area is proportional to the number of C–H bonds in the molecule times the surface excess, we estimate that the coverage of the lipids is 5.0 μmol m^{-2} (DMPC pslb in the liquid crystalline phase (L_α)) to 5.25 μmol m^{-2} (DPPC pslb in L_α). These results of the surface excess are in good agreement with the ellipsometric measurements on a lecithin bilayer adsorbed from mixed micelles of the lecithin with dodecylmaltoside [25], and with measurements of areas per molecule in bulk lamellar phases [42]. The bilayers are deposited in the L_α phase, and the surface coverage remains constant thereafter since the lipids are insoluble and the supernatant is pure water. These calculations are not exact, since the intensity of the Raman signal depends on the orientation of the molecules and the substituent groups as well as the coverage, but are sufficiently precise to confirm that the average thickness approximates to a bilayer.

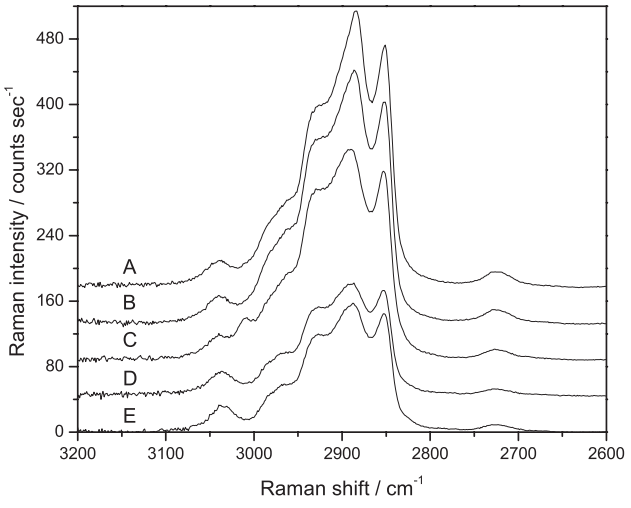

Fig. 3. Comparison of the Raman intensities of lipid bilayers with bilayer of C_{16}TAB on silica. (A) DPPC measured at 41.0 °C, (B) DMPC at 32.0 °C, (C) POPC at 32.1 °C, (D) C_{16}TAB at 34.0 °C, and (E) C_{16}TAB at 22.4 °C. S-polarized excitation, unselected axis of the detection. Spectra have been offset vertically for ease of viewing.

3.3. Polarized TIR Raman spectra

Fig. 4A and B show some of the key features of the Raman spectra of pslb's of DMPC and POPC at 20 °C with sy polarization (i.e. s-polarized incident light, y-polarized detected light, see Fig. 1B). The assignment of the peaks is well-established. The symmetric (d^+) and antisymmetric (d^-) methylene stretching vibrations of DMPC appear at 2851 and 2882 cm^{-1}, respectively [17,26]. In the bilayer of POPC, the lipid chains are more fluid and the methylene modes are consequently shifted to higher frequencies: 2855 and 2893 cm^{-1} [26,27,34]. The shoulder at 2928 cm^{-1} is assigned to a Fermi resonance of the symmetric methyl stretch (r^+_{FR}) and the peak around 2972 cm^{-1} to the antisymmetric methyl stretch (r^-) of the fatty acid chains. The antisymmetric methyl stretch of the choline head groups [17] is found at 3042 cm^{-1}. POPC also shows vinylic C–H vibrations at 3010 cm^{-1} from the oleoyl chain. In the fingerprint region (Fig. 4B), the characteristic lipid bands of DMPC (POPC) are observed: the Fermi doublet of the CH_2 scissoring mode at 1441 and 1453 cm^{-1} (1443 and 1454 cm^{-1}), the in-plane CH_2 twisting mode at 1298 cm^{-1} (1303 cm^{-1}) [27,34] and the ester carbonyl stretch at 1734 cm^{-1} (1734 cm^{-1}). Additionally, the POPC spectrum has a strong band at 1658 cm^{-1} arising from the cis carbon double bond in the oleoyl chain. The phosphate bands below 1200 cm^{-1} are obscured by the strong Si–O bands from the silica substrate.

In Fig. 4C and D, we show the four orthogonal polarizations for POPC bilayers: sx, sy, px, py, where s and p label the polarization of the pump laser and x and y the polarization of the collected Raman signal. For a uniaxial monolayer and a pump laser incident at the critical angle, θ_c, the px and py spectra should be the same (to within a scale factor due to the different transmission efficiencies of the polarization optics). Experimentally, the incident angle is about three degrees above θ_c, in order to reduce the penetration depth of the evanescent wave [30], so these two spectra are not quite identical. For isotropic layers, the sx and py spectra would be identical at all angles of

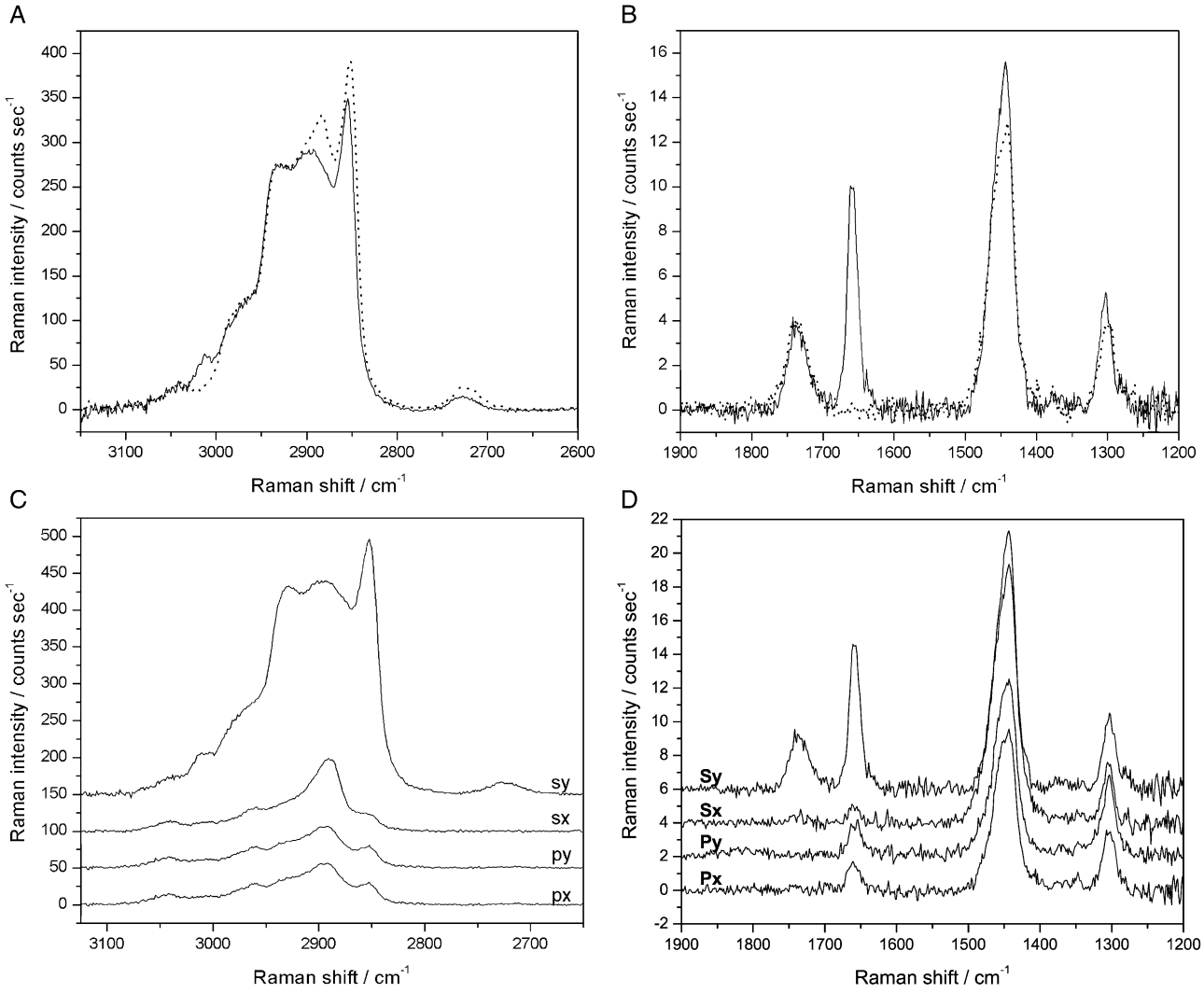

Fig. 4. Raman spectra of the pslb of DMPC (dashed lines) and POPC (solid lines) at the silica–water interface: (A) sy spectra of DMPC and POPC in the 2900 cm^{-1} region; (B) sy spectra of DMPC and POPC in the fingerprint region; (C) sy, sx, py, px spectra of POPC in the 2900 cm^{-1} region; and (D) sy, sx, py, px spectra of POPC in the fingerprint region.

incidence. While some differences are observed in the py spectrum–the symmetric methylene band is stronger and antisymmetric methylene band weaker–these results may be contrasted with the case of a crystalline layer (such as a Langmuir–Blodgett monolayer of the fatty acid, zinc arachidate) in which the CH_2 modes disappear entirely from the p-polarized spectra at the critical angle [31].

3.4. T-dependent Raman spectra

We have used TIR Raman scattering to investigate the *T* dependence of the structure of unilamellar layers of DMPC, DPPC and POPC supported on silica. In the early Raman literature, the spectra of SUVs of DMPC and DPPC in bulk solution were reported [28,29]. More recently, spectra have been recorded from single black lipid membranes [17]. To our knowledge, there have been no reports of Raman spectra from pslb's. Figs. 5, 6 and 7 show a selection of s- and p-polarized spectra of DMPC, DPPC and POPC as a function of *T*. The POPC spectra in the C–H stretching region (Fig. 7) are virtually unchanged with *T* and give an indication of how stable the experiment is over time. The DMPC and DPPC bilayers show significant *T* dependence. We will first address the qualitative features of the spectra.

Figs. 5A, B and 6A, B show the s- and p-polarized spectra in the C–H stretching region. For both lipids, the s-polarized spectra become more intense as the *T* is lowered while the p-polarized spectra become less intense. This change indicates that the axes of the hydrocarbon chains orient closer to the surface normal at lower *T*s. In both polarizations, the ratio of the intensities of the antisymmetric and symmetric methylene stretches, $I(d^-)/I(d^+)$, increases with decreasing *T* and the wavenumbers of both the d^- and d^+ modes shift to lower frequency. Both these trends are indicative of an increase in chain ordering (fewer gauche defects) at lower *T*s.

For the lipid DMPC, we have also studied the fingerprint region as a function of *T* (Fig. 5C, D and E). Fig. 5C shows

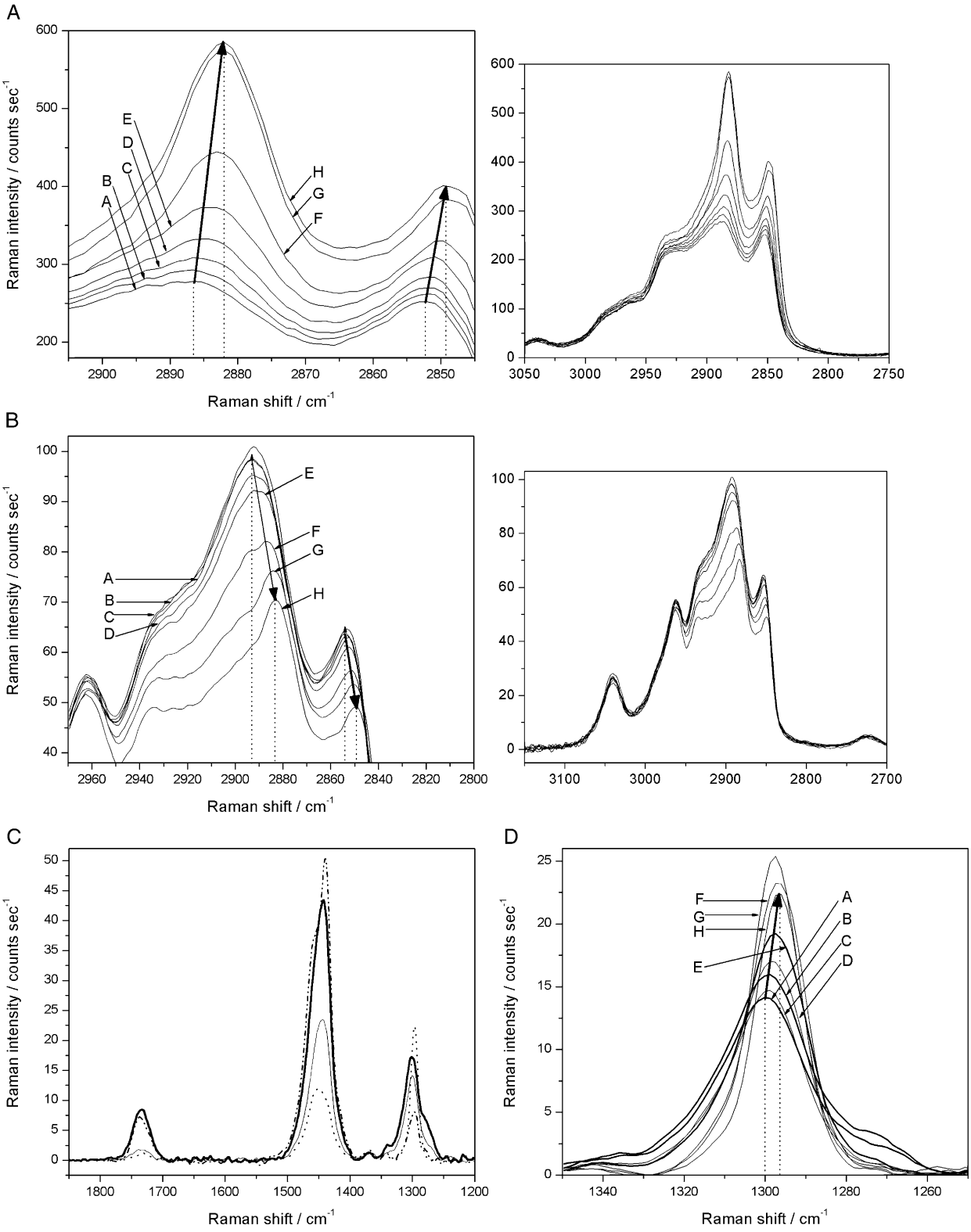

Fig. 5. Temperature (T)-dependence of the Raman spectra of a pslb of DMPC: (A) C–H stretching region, 1.2 W, s-pol, unpolarized detection and (B) C–H stretching region, 1.5 W, p-pol, unpolarized detection. Insets show full spectra; main figures show expanded region to highlight changes in intensity and peak position. Arrows indicate direction of decreasing Ts. Spectra acquired at (A) 42.0 °C, (B) 38.1 °C, (C) 32.0 °C, (D) 26.6 °C, (E) 23.3 °C, (F) 20.8 °C, (G) 16.8 °C, and (H) 13.2 °C. (C) Fingerprint region, thin solid line: p-pol, T=41.9 °C; dotted line: p-pol, T=10.5 °C; bold line: s-pol, T=41.9 °C; dash-dot line: s-pol, T=10.5 °C; laser power=1.2 W, unpolarized detection. (D) The p-pol and (E) s-pol specta of twisting mode around 1300 cm^{-1}. Arrows show the direction of decreasing Ts: (A) 41.9 °C, (B) 36.6 °C, (C) 27.5 °C, (D) 24.3 °C, (E) 22.6 °C, (F) 20.2 °C, (G) 18.1 °C, and (H) 10.5 °C; laser power of 1.2 W.

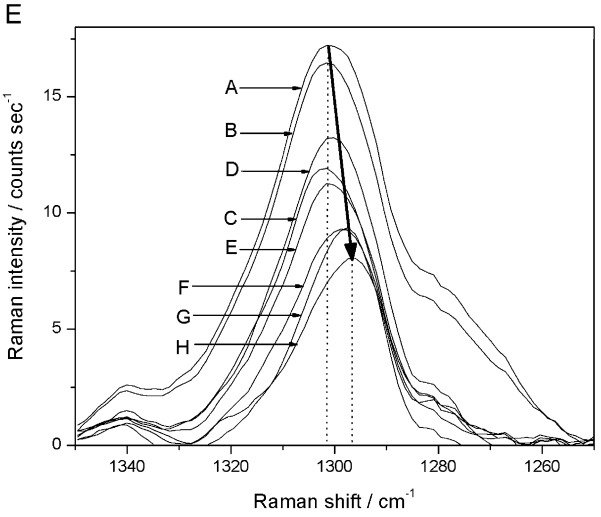

Fig. 5 (*continued*).

the s- and p-polarized spectra at 41.9 °C and 10.5 °C. The carbonyl band at 1734 cm^{-1} is little changed by *T*. In the s-polarized spectra, the CH_2 scissoring mode around 1450 cm^{-1} is slightly stronger at 10.5 °C (dash-dot line) than at 41.9 °C (bold solid line), while in the p-polarized spectra it is much weaker at 10.5 °C (dotted line) than at 41.9 °C (thin solid line). The scissoring mode involves motions of C–H bonds perpendicular to the plane of the hydrocarbon backbone. The polarizability change associated with this motion is greatest in the plane of the C–H bonds and least along the chain axis. S-polarized light probes Raman components solely in the plane of the surface, while p-polarized light predominantly samples tensor components containing the *z*-direction (normal to the surface plane). The observed intensity variations therefore indicate that the chains become more upright at lower *T*s. This inference is confirmed by the *T* dependence of the CH_2 twisting modes

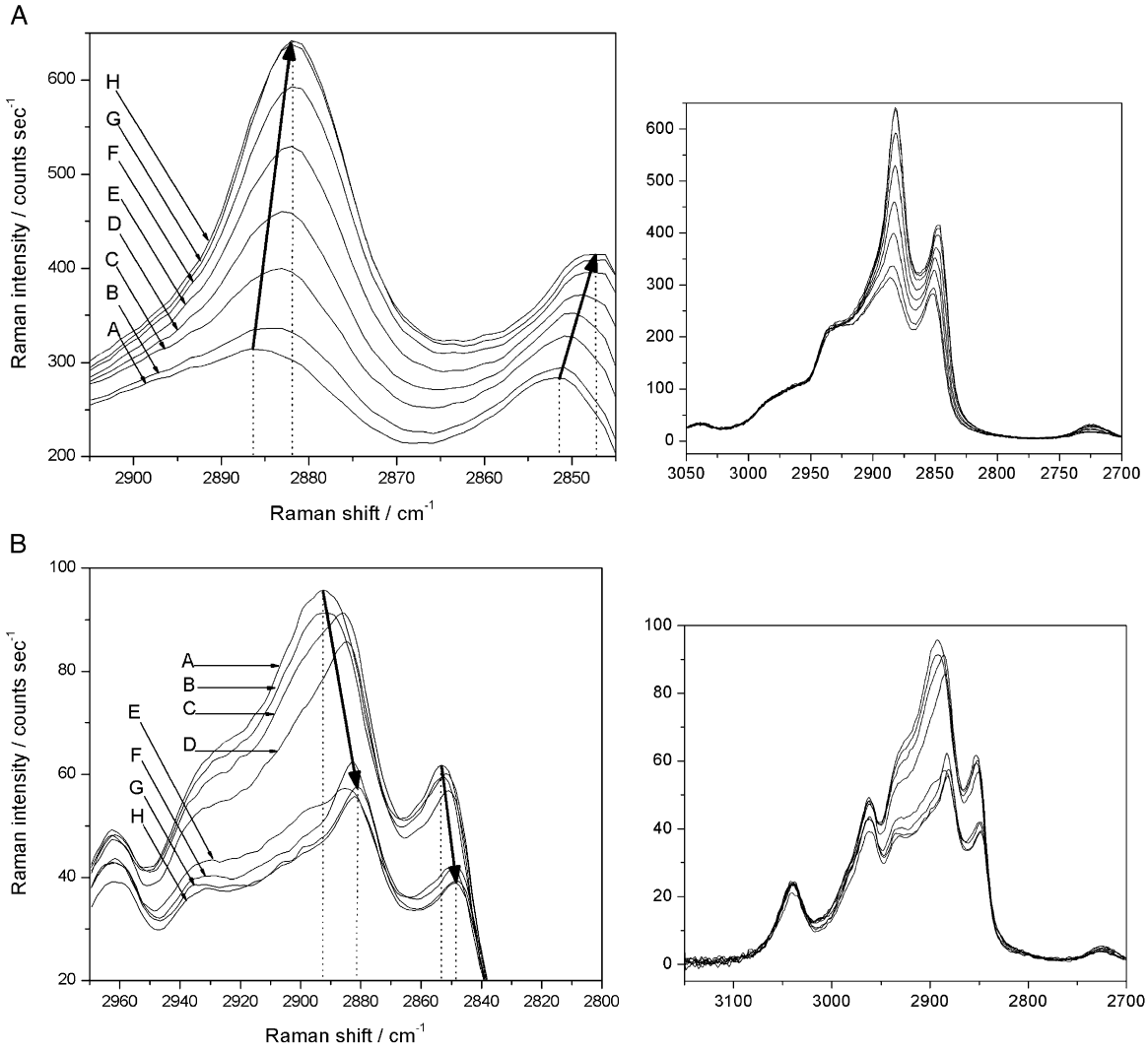

Fig. 6. *T* dependence of the Raman spectra of a pslb of DPPC: (A) C–H stretching region, 1.2 W, s-pol, unpolarized detection and (B) C–H stretching region, 1.5 W, p-pol, unpolarized detection. Insets show full spectra; main figures show expanded region to highlight changes in intensity and peak position. Arrows indicate the direction of decreasing *T*s. Spectra acquired at (A) 44.5 °C, (B) 41.0 °C, (C) 39.0 °C, (D) 37.3 °C, (E) 32.8 °C, (F) 26.8 °C, (G) 22.6 °C, and (H) 19.3 °C.

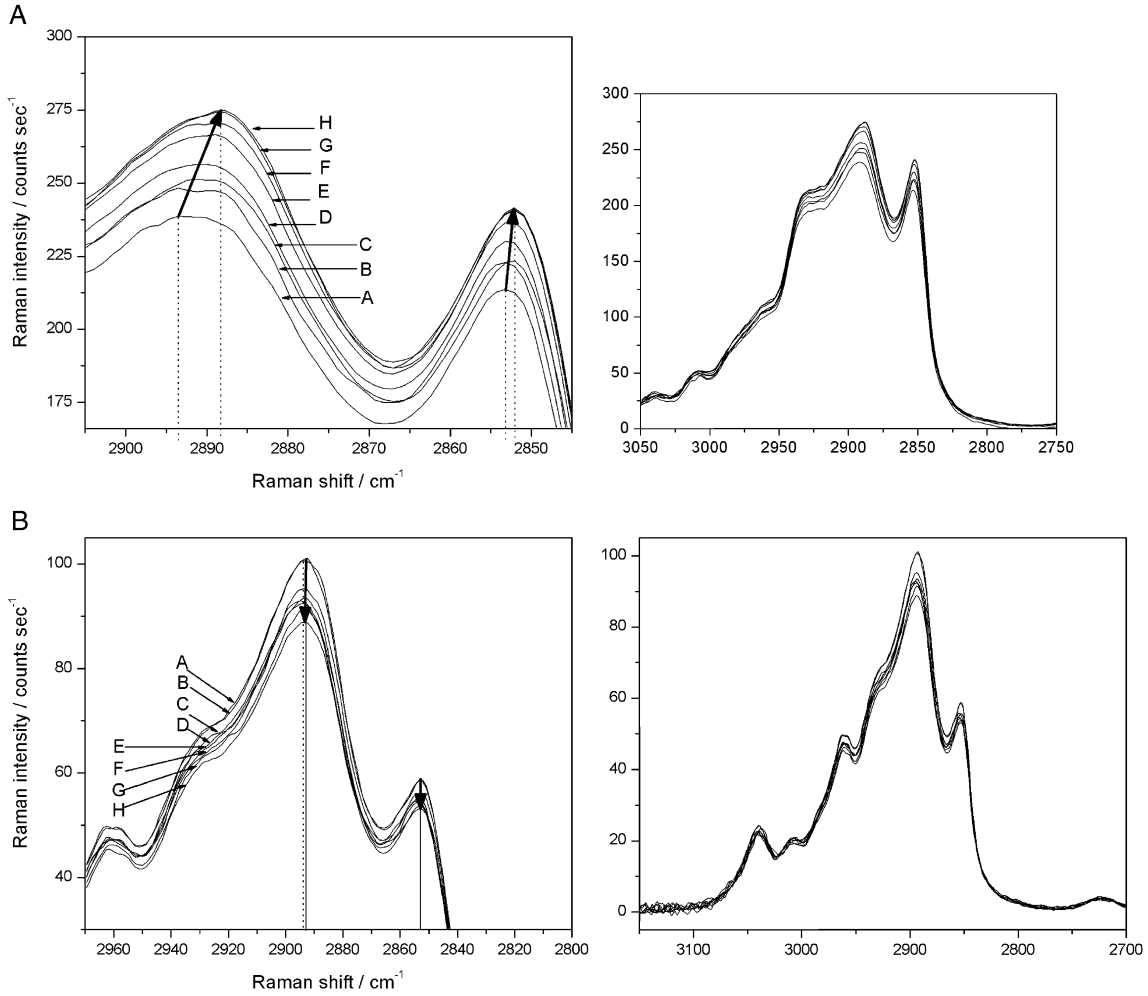

Fig. 7. *T* dependence of the Raman spectra of a pslb of POPC: (A) C–H stretching region, 1.2 W, s-pol, unpolarized detection and (B) C–H stretching region, 1.5 W, p-pol, unpolarized detection. Insets show full spectra; main figures show expanded region to highlight changes in intensity and peak position. Arrows indicate the direction of decreasing *T*s. Spectra acquired at (A) 41.0 °C, (B) 37.5 °C, (C) 32.1 °C, (D) 26.2 °C, (E) 22.9 °C, (F) 20.0 °C, (G) 17.2 °C, and (H) 13.9 °C.

around 1300 cm^{-1}. This mode is polarized predominantly along the chain axis (it corresponds to a mode assigned to B_{3g} symmetry in crystalline polyethylene [37,43]) and therefore exhibits the opposite *T* dependence to the scissoring mode. It is stronger at low *T* in the p-polarized spectrum and weaker in the s-polarized spectrum.

The twisting mode of DMPC bilayers is shown in more detail in Fig. 5D (p-polarized) and Fig. 5E (s-polarized). In addition to the variation in intensity noted above, the linewidth decreases markedly with a decrease in *T* and the frequency shifts to lower wavenumbers. The decrease in linewidth is indicative of a smaller range of conformations and/or reduced mobility in the pslb. The frequency shift is not well-documented in other lipid systems. By analogy with the C–H stretching modes, we suggest that the red-shift in the twisting mode is also a marker of increased chain ordering. Another interesting feature is the disappearance of the shoulder at 1270 cm^{-1} at lower *T*s in both polarizations. This particular peak has not been assigned with confidence,

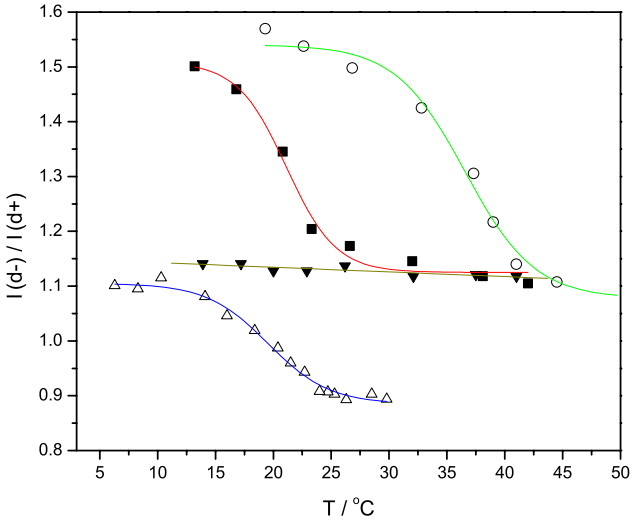

Fig. 8. Variation in $I(d^-)/I(d^+)$ with *T* for the pslb of (■) DMPC, (○) DPPC, and (▲) POPC and for (□) DMPC vesicles in a bulk suspension. Laser power=1.2 W, s-pol, unpolarized detection.

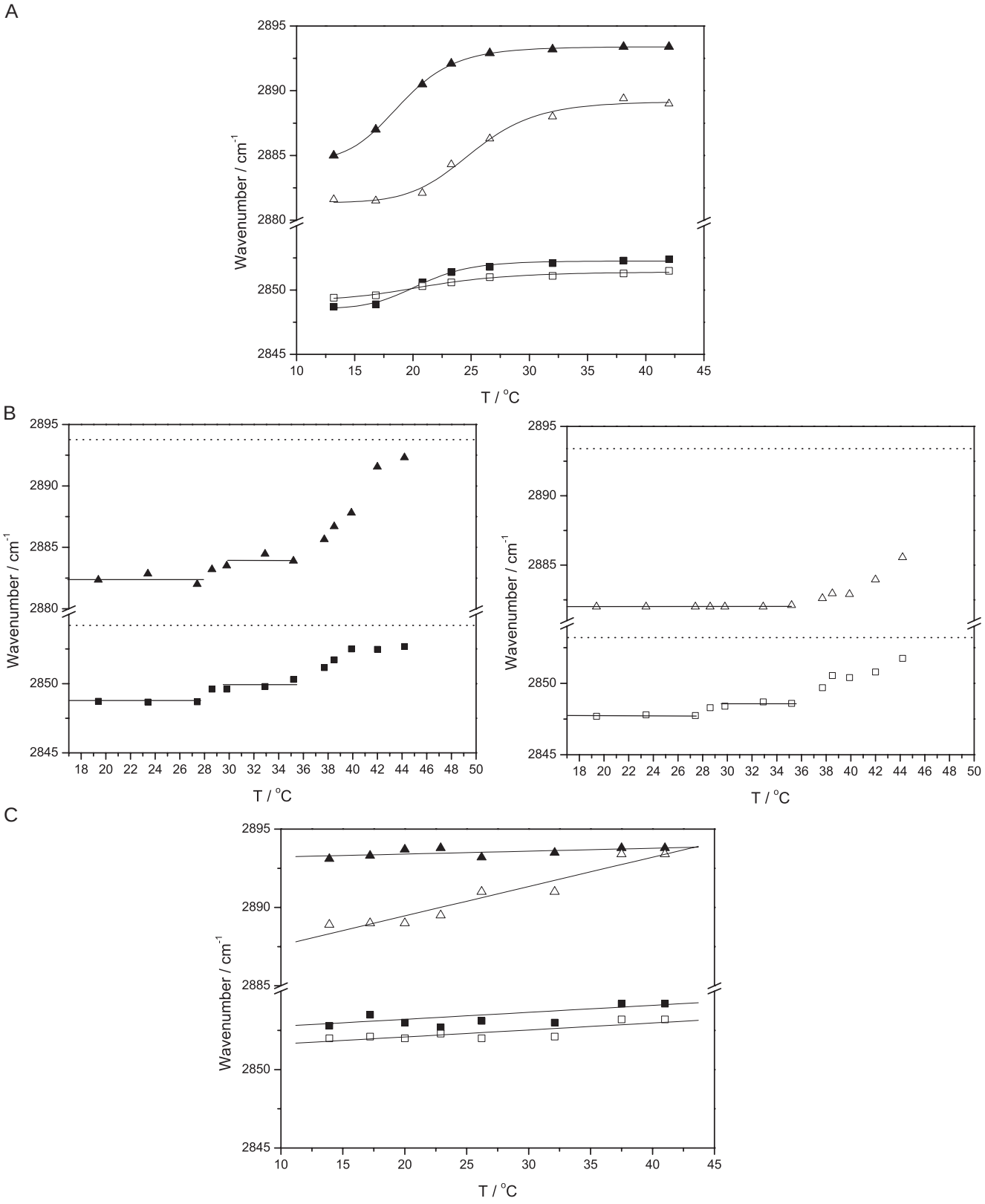

Fig. 9. The *T* dependence of the vibrational frequencies of the d^+ and d^- modes of pslb's of (A) DMPC, (B) DPPC, and (C) POPC. (▲) d^-, p-pol; (△) d^-, s-pol; (■) d^+, p-pol; (□) d^+, s-pol with unpolarized detection. The dashed lines in panel (B) indicate the wavenumbers of the POPC vibrations measured at 41.0 °C.

but it is plausible that it is associated with gauche defects, since it disappears simultaneously in both polarizations and concurrently with chain ordering as indicated by other conformational markers.

3.5. Phase transitions in the pslb's of DMPC, DPPC, and POPC

For a quantitative description of the thermotropic behavior of the pslb's, we focus on the main empirical markers of chain ordering in the Raman spectra of lipid chains: the ratio $I(d^-)/I(d^+)$ [39] and the frequencies of the CH_2 stretching modes. A higher intensity ratio and lower vibrational frequencies are indicative of increasing chain ordering. Ideally, one would deconvolute the spectra in Figs. 5–7 to obtain the linewidths and peak frequencies of the individual peaks. However, the d^- mode overlies a complex band comprising Fermi resonances of the d^+ mode with overtones of bending modes [26,35], as well as the r^+ mode of the methyl group (and its Fermi resonances), all of which may also change with *T*. Consequently, spectral decomposition cannot be undertaken with any great degree of certainty [35]. As a result we have adopted the simpler approach of fitting the regions around 2850 and 2880 cm^{-1} with a Savitzky–Golay procedure and extracting the peak intensity and peak position from these local fits. Fig. 8 shows the ratio $I(d^-)/I(d^+)$ as a function of *T* for the three lipids in pslb's. These ratios were obtained from the spectra with s-polarized excitation and unpolarized detection. Data from a bulk suspension of DMPC vesicles are also shown. Even though the polarizations of the excitation and scattering fields are the same in both experiments, the absolute value of $I(d^-)/I(d^+)$ in the bulk suspension cannot be compared directly with pslb, because the normal to the bilayer is randomly oriented in the suspension while it perpendicular to the excitation field in the pslb. Nevertheless, changes in $I(d^-)/I(d^+)$ with *T* can be correlated. For POPC bilayers, $I(d^-)/I(d^+)$ is almost constant at a value of 1.15, decreasing only very slowly with increasing *T*. Both DMPC and DPPC show the same ratio of $I(d^-)/I(d^+)$ as POPC at the highest *T*s measured. As the *T* was lowered however, $I(d^-)/I(d^+)$ increased in an approximately sigmoidal fashion, leveling out at a value of 1.5–1.6 at low *T*s. The onset of the steep part of this curve was around 41 °C for DPPC and 26 °C for DMPC. The vesicular suspension of DMPC showed very similar thermal behaviour to the pslb, but the absolute values of $I(d^-)/I(d^+)$ were much lower, ranging from 0.9 at high *T* to 1.1 at low *T*.

The frequencies of the d^+ and d^- modes of DMPC, DPPC and POPC are shown in Fig. 9(A), (B) and (C) respectively. The different vibrational frequencies recorded with s- and p-polarized excitation reflect overlap with other peaks and are not indicative of the unperturbed d^+ and d^- modes. For POPC (Fig. 9C), the frequencies increase slowly and linearly with frequency. For DMPC (Fig. 9A), the frequencies show a sigmoidal increase with frequency, the change being more pronounced in the d^- than the d^+ mode. The frequencies level out above 25 °C. For DPPC (Fig. 9B) below 28 °C, the frequencies are independent of *T*. Above 28 °C, the peak frequencies rise until at the highest *T*s measured they are within 2–3 °C of the values observed in POPC (except for the d^- mode in s-polarized spectra). The increase in frequency is not completely smooth, however, but is concentrated in the range 28–30 °C and 35–44 °C, with an indication of a plateau in-between.

4. Discussion

4.1. Benefits of TIR Raman spectroscopy

The data presented in this paper show that high-quality Raman spectra can be obtained from single planar supported lipid bilayers in an aqueous medium without the use of resonance or surface enhancement. High signal levels and the suppression of background are achieved by the use of TIR geometry for the delivery of the excitation beam. TIR-Raman has numerous attractive features. First, only material within the evanescent field contributes to the Raman spectrum, which discriminates against lipid in the bulk phase, suppresses the water signal and reduces fluorescence from chromophores in solution. Second, the electric field in an evanescent wave near the critical angle is about a factor of two larger than at normal incidence, resulting in stronger Raman spectra and shorter acquisition times. Third, higher powers can be used since the pump laser does not pass through sensitive collection optics, such as notch filters. Fourth, since there is no need to use a tightly focused laser beam to limit the depth of field, lower laser intensities can be used than in confocal Raman spectroscopy, limiting sample damage. The TIR Raman spectra reported here show a 60-fold enhancement of the signal intensity compared to published spectra of a black lipid membrane of DMPC acquired by confocal Raman microscopy [17]. (We note that benefits of the TIR geometry cannot be exploited in the black lipid experiment). Fifth, the direction of the electric field in the bilayer can be varied through the choice of the polarization of the pump laser, thus giving more structural information on the lipid and other embedded membrane constituents [20–23].

4.2. Polarized spectra indicate molecular orientation

The polarization properties of TIR-Raman scattering are well illustrated by the *T* dependence of the spectra of DMPC and DPPC in both the C–H and fingerprint regions. The s-polarized spectra sample components of the Raman tensor in the plane of the surface (α_{yy} for sy-spectra and α_{xy} for sx-spectra) while p-polarized spectra principally sample out of plane components (α_{yz} for py-spectra and α_{xz} for px-spectra). In oriented bilayers, the relative intensity of bands in these different polarizations reflects the orientation of the

molecules with respect to the surface normal. Thus the C–H stretching and scissoring modes, where the dominant change in polarizability is perpendicular to the axis of the hydrocarbon chain, are strong in s-polarized spectra for vertically oriented chains, and weak in p-polarized spectra. For the CH_2 twisting mode, where the polarizability derivative is along the chain axis, the relative intensities are reversed. All three of these bands point to a decrease in the average tilt of the hydrocarbon chains in pslb's of DMPC and DPPC with decreasing temperature.

4.3. T dependence of TIR Raman spectra of pslb's

A characteristic feature of saturated lipids is a first-order chain melting transition from a tilted 'gel' phase ($L_{\beta'}$) to a fluid 'liquid crystalline' phase (L_α). For bulk samples of hydrated lipids, this melting transition occurs at T_m=41 °C for DPPC, 23 °C for DMPC and 2 °C for POPC [33]. These calorimetric measurements show a sharp transition, with a typical width of ~2 °C. In SUVs, the main phase transition occurs at slightly lower values than in hydrated bulk phases: calorimetric measurements yielded values of T_m=38 °C for DMPC, 22 °C for DPPC and −2 °C for POPC [33]. Our Raman spectra do not show a sharp phase transition, however, either in the pslb's or in the bulk vesicular suspension, the changes occur over a T range of about 10 °C. The calorimetric phase transition T in the bulk hydrated lipids represents the onset of a gradual increase in chain ordering and untilting, as indicated by the Raman spectra. A decoupling of the thermodynamic phase transition from the conformation is not unprecedented: In the analogous phase transition in monolayers of medium-chain alcohols at the air–water interface, the melting point represents the onset of chain disordering, which then becomes greater with increasing T above T_m. We note in this regard that our experiments are conducted with a constant number of lipid molecules, so changes in the area per molecule with T will cause the physical coverage of the surface to change.

The limiting value of the ratio $I(d^-)/I(d^+)$ above the phase transition T of DMPC and DPPC is the same as that of POPC, which exists in a fluid state at all the Ts studied. With the exception of the d^- mode in s-polarized spectra, the peak frequencies of the C–H stretching modes also approach closely to that of POPC at higher Ts. Why the d^- mode should be an exception is not clear, but it may have to do with the differences between saturated and unsaturated lipids in the Fermi resonances and CH_3 modes that overlap and distort the d^- mode.

4.4. Comparison of phase transitions in pslb's and lipid vesicles of DMPC

The broadening of the phase transition observed by TIR Raman scattering from pslb's is consistent with earlier Raman spectra of SUVs of DMPC [29] and DPPC [34] in bulk suspensions. DMPC SUVs [29] showed a very smooth transition ranging from 10 °C to 27 °C, similar to our own results (Fig. 8). In contrast, literature reports of Raman spectra of large unilamellar vesicles (LUVs) showed a narrower transition range (~6 °C) and multilamellar vesicles were sharper still (~1 °C wide) [29].

The ratio of $I(d^-)/I(d^+)$, which is an established empirical measure of chain ordering, is significantly higher for pslb's than for the LUVs and SUVs of DMPC. This difference arises primarily from the different geometries of the experiments and it is difficult to separate the intrinsic contribution from geometric factors. Nevertheless, it is interesting to note that the pslb's show a much larger change in this ordering parameter than either the LUV or SUV of DMPC.

4.5. Phase transitions of pslb's of DPPC: comparison of TIR Raman scattering with other techniques

Bulk hydrated saturated lipids show an intermediate phase between the L_β and L_α, known as the ripple phase, $P_{\beta'}$. There are several reports of the existence of the ripple phase in pslb's of DPPC: DSC measurements on bilayers supported on a large number of the microscopic chips of mica [32]; measurement of the diffusion coefficient in Langmuir–Blodgett (LB) bilayers on oxidized silicon by fluorescence recovery after photobleaching (FRAP) [36]; and, recently, sum-frequency vibrational spectroscopy (SFS) of a pslb prepared by the Langmuir–Blodgett–Schaeffer method [38]. This intermediate phase may be detectable by Raman scattering in multilamellar dispersions of the DPPC [34], but has not been seen in the Raman spectra of single-bilayered vesicles despite its detection calorimetrically [40,41]. Our Raman data do not provide compelling evidence either for or against the ripple phase in pslb's of DPPC. The peak frequencies of the d^- and d^+ modes do appear to show a plateau at intermediate Ts (Fig. 9(B)), which might be taken as indicative of a third phase, but more extensive measurements would need to be taken to confirm this possibility.

5. Conclusion

We have shown in this paper that high quality Raman spectra can be acquired from pslb's in water. The method is equally applicable to fused, cushioned or tethered bilayers. The TIR geometry employed in this work enhances signals, suppresses background, reduces sample damage and provides greater polarization control than conventional confocal Raman microscopes. The clean subtraction of the water background offers significant advantages over FTIR experiments on similar systems. Recent unpublished work shows that the TIR methodology can be extended successfully to pslb's containing small peptides and consequent changes in the lipid structure can be inferred from the polarized Raman spectra. The local orientation and chain packing of the lipid

chains does not change sharply at the T of the main lipid phase transition, as reported in the literature by calorimetry. Instead, Raman spectra point to a gradual structural change over a 10 °C range below the main calorimetric phase transition. This continuous behavior has implications for experiments carried out in the gel phase of pslb's, since the local structure and dynamics may depend on T even several degrees below the calorimetric phase transition.

Acknowledgements

We thank the EPSRC and the University of Oxford for financial support. The assistance of Dr. P. Greene in the early stages of this project is gratefully acknowledged. We thank J. van Duijneveldt (Bristol) for the photon correlation measurements.

References

[1] S.A. Asher, UV resonance Raman studies of molecular structure and dynamics: applications in physical and biophysical chemistry, Annual Review of Physical Chemistry 39 (1988) 537–588.
[2] G.J. Thomas Jr., Raman spectroscopy of protein and nucleic acid assemblies, Annual Review of Biophysics and Biomolecular Structure 28 (1999) 1–27.
[3] K. Kneipp, H. Kneipp, I. Itzkan, R.R. Dasari, M.S. Feld, Surface-enhanced Raman scattering and biophysics, Journal of Physics. Condensed Matter 14 (2002) R597–R624.
[4] R. Petry, M. Schmitt, J. Popp, Raman spectroscopy—a prospective tool in the life sciences, ChemPhysChem 4 (2003) 14–30.
[5] J. Saccani, S. Castano, B. Desbat, D. Blaudez, A phospholipid bilayer supported under a polymerized Langmuir film, Biophysical Journal 85 (2003) 3781–3787.
[6] J.M. Brockman, Z. Wang, R.H. Notter, R.A. Dluhy, Effect of hydrophobic surfactant proteins SP-B and SP-C on binary phospholipid monolayers: II. Infrared external reflectance-absorption spectroscopy, Biophysical Journal 84 (2003) 326–340.
[7] C.R. Flach, J.W. Brauner, J.W. Taylor, R.C. Baldwin, R. Mendelsohn, External reflection FTIR of peptide monolayer films in situ at the air/water interface: experimental design, spectra-structure correlations, and effects of hydrogen–deuterium exchange, Biophysical Journal 67 (1994) 402–410.
[8] T. Hirschfeld, B. Chase, FT-Raman spectroscopy: development and justification, Applied Spectroscopy 40 (1986) 133–137.
[9] B. Chase, Fourier transform Raman spectroscopy, Analytical Chemistry 59 (1987) 881A–889A.
[10] K. Kneipp, H. Kneipp, I. Itzkan, R.R. Dasari, M.S. Feld, Ultrasensitive chemical analysis by Raman spectroscopy, Chemical Reviews 99 (1999) 2957–2975.
[11] G.R. Holtom, B.D. Thrall, B.Y. Chin, H.S. Wiley, S.D. Colson, Achieving molecular selectivity in imaging using multiphoton Raman spectroscopy techniques, Traffic 2 (2001) 781–788.
[12] J.-X. Cheng, S. Pautot, D.A. Weitz, X.S. Xie, Ordering of water molecules between phospholipid bilayers visualized by coherent anti-Stokes Raman scattering microscopy, Proceedings of the National Academy of Sciences of the United States of America 100 (2003) 9826–9830.
[13] L.A. Nafie, Infrared and Raman vibrational optical activity: theoretical and experimental aspects, Annual Review of Physical Chemistry 48 (1997) 357–386.
[14] J.S. Vincent, S.D. Revak, C.D. Cochrane, I.W. Levin, Interactions of model human pulmonary surfactants with a mixed phospholipid bilayer assembly: Raman spectroscopic studies, Biochemistry 32 (1993) 8228–8238.
[15] B.J. Litman, E.N. Lewis, I.W. Levin, Packing characteristics of highly unsaturated bilayer lipids: Raman spectroscopic studies of multilamellar phosphatidylcholine dispersions, Biochemistry 30 (1991) 313–319.
[16] H. Takeuchi, Y. Nemoto, I. Harada, Environments and conformations of tryptophan side chains of gramicidin A in phospholipid bilayers studied by Raman spectroscopy, Biochemistry 29 (1990) 1572–1579.
[17] F. Lhert, D. Blaudez, C. Heywang, J.-M. Turlet, Free-standing black films: an alternative to Langmuir monolayers for the study by Raman spectroscopy of peptide-phospholipid interaction in ultrathin films, Langmuir 18 (2002) 512–518.
[18] Y. Barenholz, D. Gibbes, B.J. Litman, J. Goll, T.E. Thompson, F.D. Carlson, A simple method for the preparation of homogeneous phospholipid vesicles, Biochemistry 16 (1977) 2806–2810.
[19] J. Salafsky, J.T. Groves, S.G. Boxer, Architecture and function of membrane proteins in planar supported bilayers: a study with photosynthetic reaction centers, Biochemistry 35 (1996) 14773–14781.
[20] J.M. Benevides, T. Tsuboi, J.H.K. Bamford, G.J. Thomas Jr., Polarized Raman spectroscopy of double-stranded RNA from bacteriophage phi6: local Raman tensors of base and backbone vibrations, Biophysical Journal 72 (1997) 2748–2762.
[21] S.A. Overman, M. Tsuboi, G.J. Thomas Jr., Subunit orientation in the filamentous virus Ff(fd, f1, M13), Journal of Molecular Biology 259 (1996) 331–336.
[22] M. Tsuboi, S.A. Overman, G.J. Thomas Jr., Orientation of tryptophan-26 in coat protein subunits of the filamentous virus Ff by polarized Raman microspectroscopy, Biochemistry 35 (1996) 10403–10410.
[23] C. Vigano, L. Manciu, F. Buyse, E. Goormaghtigh, J.-M. Ruysschaert, Attenuated total reflection IR spectroscopy as a tool to investigate the structure, orientation and tertiary structure changes in peptides and membrane proteins, Biopolymers 55 (2000) 373–380.
[24] R. Atkin, V.S.J. Craig, P.G. Hartley, E.J. Wanless, S. Biggs, Adsorption of ionic surfactants to a plasma polymer substrate, Langmuir 19 (2003) 4222–4227.
[25] F. Tiberg, I. Harwigsson, M. Malmsten, Formation of model lipid bilayers at the silica–water interface by co-adsorption with non-ionic dodecyl maltoside surfactant, European Biophysics Journal 29 (2000) 196–203.
[26] R.G. Snyder, H.L. Strauss, C.A. Elliger, Carbon–hydrogen stretching modes and the structure of n-alkyl chains: 1. Long, disordered chains, Journal of Physical Chemistry 86 (1982) 5145–5150.
[27] D. Aslanian, M. Negrerie, R. Chambert, A Raman spectroscopic study on the interaction of an ion-channel protein with a phospholipid in a model membrane system (gramicidin $A/_{L}$-α-lysophosphatidylcholine), European Journal of Biochemistry 160 (1986) 395–400.
[28] R.C. Spiker, I.W. Levin, Phase transitions of phospholipid single-wall vesicles and multilayers measurement by vibrational Raman spectroscopic frequency differences, Biochimica et Biophysica Acta 433 (1976) 457–468.
[29] H. Van Dael, P. Ceuterickx, J.P. Lafaut, F.H. Van Cauwelaert, The thermotropic transition of large unilamellar (LUV) vesicles of dimyristoyl phosphatidylcholine by Raman spectroscopy, Biochemical and Biophysical Research Communications 104 (1982) 173–180.
[30] P.A. Greene, C.D. Bain, Total internal reflection Raman spectroscopy, Spectroscopy Europe 16 (2004) 8–15.
[31] S. Haydock, In situ vibrational spectroscopy of thin organic films confined at the solid–solid interface. PhD thesis, University of Oxford (2002).
[32] J. Yang, J. Appleyard, The main phase transition of mica-supported phosphatidylcholine membranes, Journal of Physical Chemistry B 104 (2000) 8097–8100.

[33] R. Koynova, M. Caffrey, Phases and phase transitions of the phosphatidylcholines, Biochimica et Biophysica Acta 1376 (1998) 91–145.
[34] B.P. Gaber, W.L. Peticolas, On the quantitative interpretation of biomembrane structure by Raman spectroscopy, Biochimica et Biophysica Acta 465 (1977) 260–274.
[35] R.G. Snyder, S.L. Hsu, S. Krimm, Vibrational spectra in the C–H stretching region and the structure of the polymethylene chain, Spectrochimica Acta 34A (1978) 395–406.
[36] L.K. Tamm, H.M. McConnell, Supported phospholipid bilayers, Biophysical Journal 47 (1985) 105–113.
[37] R.G. Snyder, J.H. Schachtschneider, Vibrational analysis of the *n*-paraffins: I. Assignments of infrared bands in the spectra of C_3H_8 through *n*-$C_{19}H_{40}$, Spectrochimica Acta 19 (1963) 85–116.
[38] J. Liu, J.C. Conboy, Phase transition of a single lipid bilayer measured by sum-frequency vibrational spectroscopy, Journal of American Chemical Society 126 (2004) 8894–8895.
[39] K. Larsson, R.P. Rand, Detection of changes in the environment of hydrocarbon chains by Raman spectroscopy and its application to lipid–protein systems, Biochimica et Biophysica Acta 326 (1973) 245–255.
[40] H. Susi, J. Sampugna, J.W. Hampson, J.S. Ard, Laser-Raman investigation of phospholipids–polypeptide interactions in model membranes, Biochemistry 18 (1979) 297–301.
[41] H. Susi, D.M. Byler, W.C. Damert, Raman intensities of carbon–carbon stretching modes in a model membrane, Chemistry and Physics of Lipids 27 (1980) 337–344.
[42] L.J. Lis, M. Mcalister, N. Fuller, R.P. Rand, V.A. Parsegian, Measurement of the lateral compressibility of several phospholipids bilayers, Biophysical Journal 37 (1982) 667–672.
[43] R.G. Snyder, Interpretation of the Raman spectrum of polyethylene and deuteropolyethylene, Journal of Molecular Spectroscopy 36 (1970) 222–231.
[44] H. Schöherr, J.M. Johnson, P. Lenz, C.W. Frank, S.G. Boxer, Vesicle adsorption and lipid bilayer formation on glass studied by atomic force microscopy, Langmuir 20 (2004) 11600–11606.